

Toward a multifrequency quasi-static Ritz vector method for frequency-dependent acoustic system application

Gil Ho Yoon^{*,†}

School of Mechanical Engineering, Hanyang University, Seoul, Korea

SUMMARY

Computational issues concerning the calculation of acoustic responses of a complex finite element (FE) model for various noise and vibration inputs have become prevalent. Such a model requires a significant amount of computation time because of repeated inversions of dynamic stiffness matrices. Thus, even state-of-the-art computer hardware and software often face limitations where a model order reduction (MOR) scheme can help. The established MOR schemes such as Ritz vector or quasi-static Ritz vector methods are efficient for general engineering systems, but these MOR methods become inaccurate for frequency response analyses in some acoustic systems with frequency-dependent mass and stiffness matrices and force vectors (hereinafter frequency-dependent acoustic systems). To cope with the inaccurate prediction by these methods for frequency-dependent acoustic systems, this research presents and applies the multifrequency quasi-static Ritz vector method. Unlike the Ritz vector or quasi-static Ritz vector methods, the present multifrequency quasi-static Ritz vector method employs direct Krylov subspace bases without an orthonormal procedure at multiple center frequencies. In comparison with the existing MOR scheme, a significant gain in computational efficiency is achieved, as well as enhanced accuracy. A comparison of these methods based on criteria such as efficiency, accuracy, and reliability was also conducted. Copyright © 2011 John Wiley & Sons, Ltd.

Received 16 May 2011; Revised 15 July 2011; Accepted 7 August 2011

KEY WORDS: model reduction method; multifrequency quasi-static Ritz vector method; acoustic; Ritz vector method; quasi-static Ritz vector method

1. INTRODUCTION

Because mechanical design processes require a sequence in which ideas are introduced and iterated, it becomes challenging to calculate the acoustic and mechanical responses of complex manifold structures with fine incremental times or frequencies within a reasonable time using a state-of-the-art computer algorithm [1–4]. Reducing the number of active DOFs in finite element (FE) models is an ever-present goal across acoustic and mechanical engineering [3, 5–11]. Typically, these matters have been addressed by elaborate model order reduction (MOR) schemes such as Guyan reduction, the mode superposition (MS) method, the Ritz vector (RV) method, and the quasi-static Ritz vector (QSRV) method [1, 2, 12–15]. New MOR schemes are a topic of active research, and the concepts underlying these schemes must be validated in practical engineering problems using computational mechanics [5, 8, 13, 14, 16–25].

This research develops a so-called multifrequency quasi-static Ritz vector (MQSRV) method applicable to frequency-dependent acoustic systems that extends the frameworks of existing RV and QSRV methods that are applicable to general engineering problems [2, 15]. Frequency response analysis is a basic tool for both diagnosing processes of mechanical systems and design processes. By investigating the frequency response curve, it is possible to identify the mechanical characteristics of a system such as the existence of mechanical faults or to design the shape or topology

^{*}Correspondence to: Gil Ho Yoon, School of Mechanical Engineering, Hanyang University, Seoul, Korea.

[†]E-mail: ghy@hanyang.ac.kr

of a structure [2–4, 10, 11, 20]. For example, Figure 1 shows the sound and vibration responses of a rotating motor device consisting of coils, a stator, shaft, bearing, and supporting structures. Because of misalignments among components, bearing failures, or unknown defects of motor devices, resonance frequencies are observed in the measured acoustic and vibration signals. Resonance frequencies are typically $0.5X$, $1X$, $1.5X$ and $2X$ where X indicates the rotating frequency of the motors. The appearance of these additional resonance frequencies reflects the characteristics of existing faults (see [26] and references therein). These examples show that frequency or time domain analyses of complex manifold FE models are essential. However, even with an optimized computational solution algorithm, we face computation limitations, which only can be overcome by an MOR method that reduces the active DOFs of FE meshes but does not reduce the number of elements. As already stated, many MOR schemes have been developed so far. However, we have found that these MOR schemes may not be effective for some acoustic systems with material properties or boundary conditions that are functions of excitation frequencies. Therefore, this research is devoted to the development of the MQSRV method, which provides a considerably more accurate prediction of acoustic response than the common MOR methods in the presence of frequency-dependent acoustic stiffness and mass matrices.

The existing MOR methods are effective for almost all structural and acoustic problems [24]. However, we note that some particular situations arise in which standard MOR schemes are difficult to apply. In particular, it becomes difficult to apply the standard MOR methods, which are developed for constant stiffness and mass matrices and force vectors, to frequency-dependent acoustic and structure systems with frequency-dependent mass and stiffness matrices and force vectors. For example, the frequency-dependent mixed boundary condition, that is, the Sommerfeld boundary condition [27], and the absorptive material inevitably make the frequency-dependent mass and stiffness matrices and the force vector dependent on frequency. In this particular case, numerical

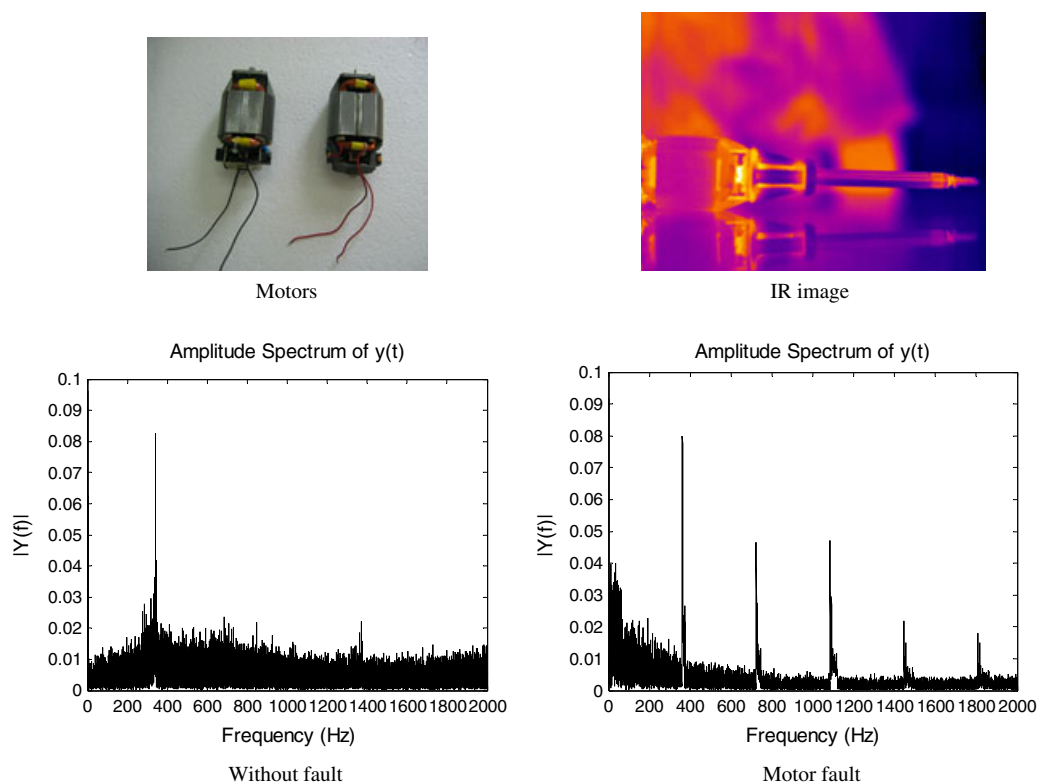


Figure 1. Acoustic system example. A rotating device (Depending on the origins of faults, special rules with respect to resonance frequencies are observed. It is important to compare the responses of the FE model and experiments to understand the origins of faults in systems of interest.)

observation shows that using the existing MOR scheme is not favorable because an accurate calculation of an approximate solution is not possible. To resolve these adverse effects by extending the concepts of the RV method and the QSRV method, we present a new MOR method: the MQSRV method. This new MOR method is based on the QSRV method proposed by Gu *et al.* in 2000. This method calculates its bases at multiple frequencies in contrast to conventional MOR methods, which calculate their bases at one center frequency. This kind of expansion is not new to the MOR method, but to our knowledge, this study is the first to present the concept of calculating bases at multiple frequencies for a frequency-dependent acoustic system. Additionally, we found that the orthonormal step of the RV and QSRV methods can be omitted from an engineering point of view.

The layout of the paper is as follows. First, some MOR schemes, such as the RV method and the QSRV methods, are introduced and their essential concepts are explained. The MQSRV method, which has many similarities with the QSRV method for multifrequency domains, is developed. Using some analysis benchmark examples of two-dimensional (2D) and three-dimensional (3D) complex acoustic problems, the efficiency and characteristics of the present MQSRV method are numerically studied and compared. Finally, our findings and some topics for future research are summarized and discussed in the conclusion.

2. FORMULATIONS FOR FREQUENCY-DEPENDENT ACOUSTIC SYSTEMS

Because absorption and attenuation of the pressure field are observed with intrinsically absorptive materials such as fibers, wood, and carbon particles, complex material models are often adopted for realistic acoustic simulations. This statement also can be applied to mechanical wave and electromagnetism problems where their governing equations are the Helmholtz equation [28]. For another example of frequency-dependent system, the elastic susceptibility of viscoelastic material is also parameterized by the complex shear modulus depending on the frequency of excitation force [29, 30]. Even without sound-absorptive materials that have complex wave numbers and density values, a set of equations in FEM or finite difference method (FDM) often becomes frequency-dependent because of a complex impedance boundary condition such as the Sommerfeld boundary condition [27, 28]. Furthermore, calculation of the responses on the basis of these conditions and materials at a wide range of frequencies of interest inevitably requires many time-consuming inversions of complex matrices [4, 17]. For these reasons, we utilize the concept of MOR schemes to develop a new method called MQSRV.

In ideal incompressible (low Mach number) fluid flow, neglecting the existence of viscosity and the absorption and attenuation because of the viscosity, the governing equation for the harmonically varying pressure, that is $\tilde{p}(t) = p e^{i\omega t}$, in an acoustic medium, Ω_a , is given as follows:

$$\text{Helmholtz equation: } \nabla \cdot \left(\frac{1}{\rho} \nabla p \right) + \frac{\omega^2 p}{\rho c^2} = 0, \quad \left(k = \frac{\omega}{c} \right) \quad \text{on } \Omega_a \quad (1)$$

where p , ρ , and c are the pressure in the acoustic domain Ω_a , the complex density of the acoustic domain, and the local speed of sound, respectively. The angular velocity and the complex wave number are denoted by ω and k , respectively.

The specific acoustic impedance, Z , is defined as the ratio of the acoustic pressure to the associated fluid speed (u) as follows [28]:

$$Z = p/u = R_z + X_z i, \quad (2)$$

where R_z and X_z are the specific acoustic resistance and the specific acoustic reactance of the acoustic medium, respectively. By confining our consideration to ideal nondissipative wave propagation, Z becomes ρc .

The pressure field is obtained by solving the above Helmholtz equation with proper boundary conditions. This paper considers the following four types of boundary conditions:

$$\text{Pressure boundary condition: } p = p_0 \quad (3a)$$

$$\text{Hard wall condition: } \mathbf{n} \cdot \nabla p = 0 \quad (3b)$$

$$\text{Acceleration boundary condition: } \mathbf{n} \cdot \nabla p = a_n \quad (3c)$$

$$\text{Sommerfeld boundary condition: } \mathbf{n} \cdot \nabla p + i \cdot k \cdot p = 2i \cdot k \cdot p_{\text{in}} \quad (3d)$$

where p_0 , \mathbf{n} , a_n , and p_{in} are the input pressure, the outward unit normal to the fluid medium, the input acceleration, and the pressure amplitude of an incoming wave, respectively. For simulation of the wave propagation boundary condition without reflection (anechoic termination after an acoustic device), the Sommerfeld boundary condition (3d) is applied with $p_{\text{in}} = 0$. As stated before, because of the complex terms in the Sommerfeld boundary condition, the resulting set of equations becomes frequency-dependent.

2.1. Complex material: Delany–Bazley material

The conventional wave Equation (1) is derived under the assumption that all the losses of acoustic energy can be neglected. In this ideal situation, the dissipation of acoustic energy is small enough to neglect the effect of the dissipation on the acoustic wave flow. However, in some practical situations, energy dissipation from the absorption and attenuation of sound cannot be neglected and should be considered in computational simulation [29–31]. To consider the effect of sound-absorptive materials on acoustic pressure, the Delany–Bazley material model, which is an empirical formulation for porous absorbing materials such as fiber and wood, is considered during some of the simulations conducted in the next section as follows:

$$k_c = k_a \left(1 + 0.0978 \left(\frac{\rho_a f}{R} \right)^{-0.7} - i 0.189 \left(\frac{\rho_a}{f} R \right)^{-0.595} \right) \quad (4a)$$

$$Z_c = Z_a \left(1 + 0.057 \left(\frac{\rho_a f}{R} \right)^{0.734} - i 0.087 \left(\frac{\rho_a f}{R} \right)^{-0.732} \right) \quad (4b)$$

$$c_c = \frac{\omega}{k_c}, \rho_c = k_c Z_c / \omega, f = \frac{\omega}{2\pi}, \quad (4c)$$

where the wave number and the density of air without attenuation are denoted by k_a and ρ_a , respectively. The complex wave number and impedance of the Delany–Bazley empirical material model are k_c and Z_c , respectively. The coefficient of the flow resistivity is R and is commonly measured by experiment [32]. Besides the empirical formulation derived by Delany and Bazley, other empirical material models have recently been proposed by Mike [31] and Allard and Champoux [33]. To show the advantage of the MQSRV method developed in the next section, only the above Delany–Bazley material model is considered, but the other material models can also be applied. The significant difference of the Delany–Bazley empirical formulation is that the resulting mass and stiffness matrices and the force vector become frequency-dependent. From a FEM point of view, the sound speed and the density in (1) are substituted by the complex sound speed and the derived density of Equation (4c).

After formulating the finite element with complex materials and the complex boundary condition, the following matrix form can be written without loss of generality:

$$[-\omega^2 \mathbf{M}(\omega) + \mathbf{K}(\omega)] \mathbf{X} = \mathbf{F}(\omega). \quad (5)$$

The pressure vector and the force vector are denoted by \mathbf{X} and \mathbf{F} , respectively, in the context of the finite element procedure. The frequency-dependent stiffness and mass matrices are denoted by \mathbf{K} and \mathbf{M} , respectively.

3. DEVELOPMENT OF A MULTIFREQUENCY QUASI-STATIC RITZ VECTOR METHOD

3.1. Introduction to the model reduction scheme

With the advent of highspeed parallel computers and solution algorithms for FE procedures, FE has become a very powerful tool for engineers who analyze and design complex continuum structures

[17]. It has become possible to increase the number of finite elements for accurate response calculations for continuum structures. However, we can easily imagine simulation cases with FE meshes that are too fine and cannot be solved by the most advanced, state-of-the-art system within a moderate computation time. Design engineers must consider inherent limitations in computational speed and hardware capacity. These limitations often can be mitigated by the introduction of an MOR scheme, which reduces the size of assembled stiffness matrices but still provides accurate solutions [1, 2, 4, 9–11, 24, 34]. Various model reduction schemes such as Guyan reduction, mode superposition, Ritz vector, modal acceleration and quasi-static Ritz vector methods have been developed in computational mechanics and are widely used in commercial software. Along with Krylov subspace methods and Guyan reduction, there is a method called proper orthogonal decomposition, which was developed for CFD applications (see [25] and references therein). Except for the Guyan reduction scheme, other model reduction schemes share similarities in the way they reduce the system size. Basically, they transform a large set of system equations into a small set of equations by approximating the original structural response with the approximated response, $\Psi\mathbf{Q}$. Thus, the approximated response, \mathbf{X}_A , of the original response \mathbf{X} can be defined as follows:

$$\mathbf{X} \cong \mathbf{X}_A = \Psi\mathbf{Q} \quad (6)$$

$$\Psi = [\varphi_1, \varphi_2, \dots, \varphi_{n_d}](n_d \leq n), \quad (7)$$

where \mathbf{Q} is the frequency dependent vector of order n_d and Ψ is the retained set of the considered orthonormal basis φ_i . By premultiplying Ψ^T into the original dynamic Equation (5), the following reduced equation with order n_d is obtained:

$$\underbrace{\{\Psi^T [-\omega^2 \mathbf{M}(\omega) + \mathbf{K}(\omega)] \Psi\}}_{n_d \times n_d} \underbrace{\mathbf{Q}}_{n_d \times 1} = \underbrace{\Psi^T \mathbf{F}(\omega)}_{n_d \times 1}. \quad (8)$$

By solving the above reduced system with order n_d for \mathbf{Q} , the approximate solution \mathbf{X}_A is recovered using Equation (6). In MOR methods, it is common to use a small number of bases ($n_d \ll n$) that results in approximated frequency responses. As stated before, depending on the choice of Ψ (the response choice depends on the engineering application), a number of schemes have been developed. In the following sections, only the basic concept and formulations of the RV method and the QSRV method are discussed because the MQSRV method presented later is based on the concepts of the two MOR methods.

3.2. The Ritz vector method and the quasi-static Ritz vector method

The RV method and the QSRV method construct their reduction bases Ψ by considering the external force \mathbf{F} , the mass matrix \mathbf{M} , and the stiffness matrix \mathbf{K} [2, 4, 9]. From a mathematical point of view, they generate the Krylov subspace for their bases. The order n Krylov subspace κ_n generated by a matrix \mathbf{A} and a vector \mathbf{b} is the linear subspace as follows:

$$\kappa_n(\mathbf{A}, \mathbf{b}) = \text{span}\{\mathbf{b}, \mathbf{A}\mathbf{b}, \mathbf{A}^2\mathbf{b}, \dots, \mathbf{A}^{n-1}\mathbf{b}\}. \quad (9)$$

Because the calculated Krylov subspace bases are almost linearly dependent on each other, the use of an orthogonalization procedure such as Arnoldi iteration is common [2–4, 9]. During the orthogonalization procedure, matrix \mathbf{A} and vector \mathbf{b} are mathematically constant.

On the basis of the Krylov subspace of (9), the first basis, φ_1 , is constructed by solving the static equation and normalizing the static displacement to the mass matrix in the RV method and the QSRV method as follows:

$$\varphi_1 = \frac{1}{\varphi_1^{*T} \mathbf{M} \varphi_1^*} \varphi_1^*, \quad \varphi_1^* \equiv (\mathbf{K}(\omega_c) - \omega_c^2 \mathbf{M}(\omega_c))^{-1} \mathbf{F}(\omega_c). \quad (10)$$

The next bases are sequentially constructed from the following equations:

$$\varphi_j^* \equiv (\mathbf{K} - \omega_c^2 \mathbf{M})^{-1} (\mathbf{M} \varphi_{j-1}) \quad (11)$$

$$\text{Orthogonalization: } \boldsymbol{\varphi}_j^{**} \equiv \boldsymbol{\varphi}_j^* - \sum_{k=1}^{j-1} (\boldsymbol{\varphi}_k^{*T} \mathbf{M} \boldsymbol{\varphi}_k) \boldsymbol{\varphi}_k \quad (12)$$

$$\text{Normalization: } \boldsymbol{\varphi}_j = \frac{1}{\boldsymbol{\varphi}_j^{**T} \mathbf{M} \boldsymbol{\varphi}_j^{**}} \boldsymbol{\varphi}_j^{**}, \quad (13)$$

where $\boldsymbol{\varphi}_j$ with the right superscript (*) and (**) denote the two auxiliary variables for the j -th basis. The center frequency of interest is denoted by ω_c [2, 4, 5]. With zero center frequency, the above method becomes the RV method. Note that the previously calculated bases are used to make a new basis orthogonal to them. To avoid computing the inverse of the dynamic stiffness matrix in the repeated constructions of the reduction bases, the LU decomposition method or similar methods are commonly employed in Equations (10) and (11). More computer memory is needed for the upper and lower triangular matrices and the associated computational time, but the computational advantages of the alternate methods can compensate for these additional bundles. The reduction in bases depends on how accurately we want to approximate the responses of a dynamic structure.

After building the bases, the structural response \mathbf{X} is approximated by

$$\mathbf{X} \cong \mathbf{X}_A = \boldsymbol{\Psi} \mathbf{Q}. \quad (14)$$

One distinct point of these methods compared with the MS method is that they generate the reduction bases $\boldsymbol{\Psi}$ by considering not only the mass and stiffness matrices of dynamic structures, but also the external applied forces.

To explain aspects of this approach further, we again consider the concept of the Krylov subspace.

First, let us consider a linear system, that is, a frequency-independent acoustic system, as follows:

$$\underbrace{[\mathbf{K}_c]}_{\text{Constant}} - \omega^2 \underbrace{[\mathbf{M}_c]}_{\text{Constant}} \mathbf{X} = \underbrace{[\mathbf{F}_c]}_{\text{Constant}}. \quad (15)$$

The right subscript c indicates that a matrix or a force with this subscript is constant. Bearing in mind that the stiffness matrix \mathbf{K}_c , the mass matrix \mathbf{M}_c and the force vector \mathbf{F}_c are constants with respect to the angular velocity, the response, \mathbf{X} , can now be expanded around an expansion point, ω_c , in a Taylor's expansion.

$$[\mathbf{K}_c - \omega_c^2 \mathbf{M}_c + (\omega^2 - \omega_c^2) \mathbf{M}_c][\mathbf{X}_0 + (\omega^2 - \omega_c^2) \mathbf{X}_1 + (\omega^2 - \omega_c^2)^2 \mathbf{X}_2 \cdots] = \mathbf{F}_c, \quad (16)$$

where \mathbf{X}_i denotes the moments of the Taylor's expansion. By collecting the terms according to the powers of $(\omega^2 - \omega_c^2)$, which are called *moments*, and equating these terms, the recursive condition can be derived as shown below. It is worth noting that the *moments* after the orthonormal procedure become the Krylov subspace bases of the QSRV method.

$$[\mathbf{K}_c - \omega_c^2 \mathbf{M}_c] \mathbf{X}_0 = \mathbf{F}_c \quad (17)$$

$$[\mathbf{K}_c - \omega_c^2 \mathbf{M}_c] \mathbf{X}_i = -\mathbf{M}_c \mathbf{X}_{i-1} \text{ or } \mathbf{X}_i = -[\mathbf{K}_c - \omega_c^2 \mathbf{M}_c]^{-1} \mathbf{M}_c \mathbf{X}_{i-1} \text{ for } i = 1, 2, 3 \cdots \quad (18)$$

After solving the above equations, it is obvious that the original response \mathbf{X} can now be expanded.

$$\mathbf{X}(\omega) = \mathbf{X}_0 + (\omega^2 - \omega_c^2) \mathbf{X}_1 + (\omega^2 - \omega_c^2)^2 \mathbf{X}_2 \cdots \quad (19a)$$

$$\text{or } \mathbf{X}(\omega) = c_0(\omega) \mathbf{X}_0 + c_1(\omega) \mathbf{X}_1 + c_2(\omega) \mathbf{X}_2 \cdots \quad (19b)$$

where c_i are the constant coefficients for constructing the response \mathbf{X} . Not surprisingly, the above expansion theory is fundamental to the RV and QSRV methods. From the above explanations, it is definitely true that the choice of the center frequency is very important. In other words, the best approximation can be achieved near the center frequency. Therefore, the Krylov subspace method is relatively insensitive to eigenfrequency compared with the mode superposition method. For more details, see [2, 14, 15].

3.3. Present multifrequency quasi-static Ritz vector method

The above RV and QSRV methods are developed for a frequency-independent system with a constant mass matrix, stiffness matrix, and force vector. However, as shown in the previous section, with a complex boundary condition and porous material, the resulting FE matrices and force vector become frequency-dependent, which may make the two MOR methods inefficient. Theoretically, the Krylov subspace bases of (9) should not be applied to a frequency-dependent system. Therefore, based on this estimable QSRV method developed in [2, 4], this section is devoted to developing a simple but efficient MOR approach that is applicable to a frequency-dependent acoustic system.

Note that standard RV and QSRV methods include an orthonormal procedure to improve the mathematical properties of the bases. Recalling that these methods are developed using Krylov subspace bases, it is evident that, in principle, an orthonormal procedure can be omitted as follows:

$$\text{Alternative QSRV method: } \boldsymbol{\varphi}_1 \equiv \underbrace{(\mathbf{K})}_{\text{Constant}} - \omega_c^2 \underbrace{(\mathbf{M})}_{\text{Constant}})^{-1} \underbrace{(\mathbf{F})}_{\text{Constant}} \quad (20)$$

$$\boldsymbol{\varphi}_j \equiv (\mathbf{K} - \omega_c^2 \mathbf{M})^{-1} (\mathbf{M} \boldsymbol{\varphi}_{j-1}) \quad (21)$$

$$\omega_c (= \frac{\omega_{\text{start}} + \omega_{\text{end}}}{2}) \quad j = 1, \dots, n_d. \quad (22)$$

Note that the above procedures produce Krylov subspace bases with order n_d . We note that from a mathematical point of view, the generated bases of the standard RV and QSRV methods and the alternative RV method should represent the same vector spaces if truncation errors can be neglected.[‡]

Here, we further question the usage of the *one* center frequency. Note that the Ritz bases of the alternative RV method from (20) to (22) are best around the center frequency. For most numerical cases, approximation near the center frequency is sufficient. However, we found that consideration of multiple center frequencies (more than one for several frequency domains) is possible; a similar observation was already made [2, 15]. In [2], the Ritz vectors are generated with multiple center frequencies where in [15], the bases of the mode superposition method are generated with multiple center frequencies. Therefore, the alternative QSRV method can be modified as follows:

$$\boldsymbol{\varphi}_{s,1} \equiv (\mathbf{K}(\omega_{c,s}) - \omega_{c,s}^2 \mathbf{M}(\omega_{c,s}))^{-1} \mathbf{F}(\omega_{c,s}) \quad (23)$$

$$\boldsymbol{\varphi}_{s,j} \equiv (\mathbf{K}(\omega_{c,s}) - \omega_{c,s}^2 \mathbf{M}(\omega_{c,s}))^{-1} (\mathbf{M}(\omega_{c,s}) \boldsymbol{\varphi}_{s,j-1}) \quad (24)$$

$$\omega_{c,s} (= \frac{\omega_{s,\text{start}} + \omega_{s,\text{end}}}{2}), \quad s = 1, \dots, nf, \quad j = 1, \dots, n_{d,s}, \quad (25)$$

where the starting frequency, the ending frequency, and the center frequency of the s -th frequency domain are denoted by $\omega_{s,\text{start}}$, $\omega_{s,\text{end}}$, and $\omega_{c,s}$, respectively, where the total number of considered

[‡]One of the computational advantages of direct usage of Krylov subspace bases is that the computation cost of the orthonormal procedure can be avoided.

frequency domains is nf . The number of bases calculated for the s -th frequency domain is denoted by $n_{d,s}$. Although almost all the procedures are the same as those proposed in [1], the stiffness and mass matrices and the force vector are dependent on the angular speed. The orthonormalization procedure is not applied because of the frequency-dependent mass matrix used to normalize the calculated auxiliary vectors. Finally, using the above simplified procedure, the following bases are calculated:

$$\mathbf{Q} = [\underbrace{\varphi_{1,1} \cdots \varphi_{1,n_{d,1}}}_{\text{the 1st domain}}, \underbrace{\varphi_{1,2} \cdots \varphi_{1,n_{d,2}}}_{\text{the 2nd domain}}, \cdots, \underbrace{\varphi_{1,nf-1} \cdots \varphi_{1,n_{d,nf-1}}}_{\text{the } nf-1 \text{ domain}}, \underbrace{\varphi_{1,nf} \cdots \varphi_{1,n_{d,nf}}}_{\text{the } nf \text{ domain}}]. \quad (26)$$

Notwithstanding the fact that the MQSRV method is very simple to implement and use, it is very effective in a frequency-dependent acoustic system. To explain aspects of this approach further, we need to revisit the usage of the Krylov subspace for frequency-dependent acoustic systems.

Let us consider a frequency-dependent acoustic system in Equation (5). By only imposing the Sommerfeld boundary condition, the mass matrix and the force vector are modified as follows (see [28] and [35] for the actual FEM implementation code):

$$[\mathbf{K}_c - (\omega^2 \mathbf{M}_c + \omega \mathbf{M}_s)] \mathbf{X} = \mathbf{F}_c + \omega \mathbf{F}_s, \quad (27)$$

where \mathbf{M}_s and \mathbf{F}_s are the additional mass matrix and force vector formulated from the acoustic FE implementation of the Sommerfeld boundary condition [35]. Similar to (16), we can expand Equation (27).

$$\omega = \omega_c + \frac{(\omega^2 - \omega_c^2)}{2\omega_c} - \frac{(\omega^2 - \omega_c^2)^2}{8} \omega_c^{-3/2} \cdots (\text{Taylor's series}) \quad (28a)$$

$$\begin{aligned} & \left[\mathbf{K}_c - \omega_c^2 \mathbf{M}_c - (\omega^2 - \omega_c^2) \mathbf{M}_c - \left[\omega_c + \frac{(\omega^2 - \omega_c^2)}{2\omega_c} - \frac{(\omega^2 - \omega_c^2)^2}{8} \omega_c^{-3/2} \cdots \right] \mathbf{M}_s \right] \\ & \times [\mathbf{X}_0 + (\omega^2 - \omega_c^2) \mathbf{X}_1 + (\omega^2 - \omega_c^2)^2 \mathbf{X}_2 \cdots] \\ & = \mathbf{F}_c + \left[\omega_c + \frac{(\omega^2 - \omega_c^2)}{2\omega_c} - \frac{(\omega^2 - \omega_c^2)^2}{8} \omega_c^{-3/2} \cdots \right] \mathbf{F}_s \end{aligned} \quad (28b)$$

By collecting the terms from Equation (28b) according to the powers of $(\omega^2 - \omega_c^2)$, the following equations can be obtained:

$$\begin{aligned} & [\mathbf{K}_c - \omega_c^2 \mathbf{M}_c - \omega_c \mathbf{M}_s] [\mathbf{X}_0] = \mathbf{F}_c + \omega_c \mathbf{F}_s \text{ for the zeroth order term} \\ & \left(-\mathbf{M}_c - \frac{1}{2\omega_c} \mathbf{M}_c \right) \mathbf{X}_0 + (\mathbf{K}_c - \omega_c^2 \mathbf{M}_c - \omega_c \mathbf{M}_s) \mathbf{X}_1 = \frac{1}{2\omega_c} \mathbf{F}_s \text{ for the first order term} \\ & (\mathbf{K}_c - \omega_c^2 \mathbf{M}_c - \omega_c \mathbf{M}_s) \mathbf{X}_2 - \left(\mathbf{M}_c + \frac{1}{2\omega_c} \mathbf{M}_s \right) \mathbf{X}_1 + \frac{\omega_c^{-3/2}}{8} \mathbf{M}_s \mathbf{X}_0 = -\frac{\omega_0^{-3/2}}{8} \mathbf{F}_s \\ & \text{for the second order term and so on.} \end{aligned} \quad (29)$$

Using the calculated moments in (29), the following approximation is also possible:

$$\mathbf{X}(\omega) = \mathbf{X}_0 + (\omega^2 - \omega_c^2) \mathbf{X}_1 + (\omega^2 - \omega_c^2)^2 \mathbf{X}_2 \cdots \quad (30)$$

The above complex relationships of Equation (29) prove that direct use of the Krylov subspace is improper from a mathematical point of view. Such use violates the basic hypothesis of the Krylov subspace. Furthermore, by considering absorptive acoustic materials such as the Delany–Bazley material, it seems almost impossible to derive a simple recursive condition for moments. Nevertheless, it is our proposition to use combinations of the Krylov subspaces directly calculated at multiple center frequencies without an orthonormal procedure as in (26). Although this idea is simple, it is very effective. See the Appendix for the orthogonality of the present MQSRV method.

4. NUMERICAL EXAMPLES

To verify the accuracy and numerical characteristics of the present MQSRV method compared with existing MOR methods, this section contains several illustrative acoustic examples. As mentioned before, the considered acoustic systems are characterized by the dependency of the mass and stiffness matrices and the force vector at the excitation frequency.

4.1. Example 1: acoustic example (2D muffler)

Consider the transmission loss (TL) of a muffler structure with an expansion chamber for noise attenuation shown in Figure 2. At the inlet tube of the left side and the outlet tube of the right side, the Sommerfeld boundary conditions are imposed for the incoming wave and the outgoing wave without reflection, respectively. Because the characteristics of this two-dimensional muffler are well studied in the literature [36], it was chosen to prove the validity and efficiency of the present approach. The TL curve can be computed by the three-points method, which involves calculating the approximate transmission loss using the pressures at the three points in Figure 2 [36]. First, assuming a one-dimensional acoustic wave at the inlet tube, the magnitude of the incoming wave pressure is approximated by Equation (31).

$$p_i = \frac{1}{e^{ikx_1}} \frac{p_1 - p_2 e^{-ikx_{12}}}{1 - e^{-i2kx_{12}}} (p_1 = p_i e^{ikx_1} + p_r e^{-ikx_1}, p_2 = p_i e^{ikx_2} + p_r e^{-ikx_2}), \quad (31)$$

where p_1 and p_2 are the complex pressures at two arbitrary points of the inlet tube (Figure 2(a)) and the distance between the two points ($x = x_1, x = x_2$) is $x_{12} (= x_2 - x_1)$ as shown in Figure 2(a). The magnitudes of the incoming wave and the reflected wave are denoted by p_i and p_r , respectively. The transmission loss of the acoustic muffler can be approximately evaluated from the ratio of the incoming wave pressure to the transmitted wave pressure by the following equation:

$$TL = 20 \log \left(\left| \frac{p_i}{p_3} \right| \right) + 10 \log \left(\left| \frac{A_i}{A_o} \right| \right), \quad (32)$$

where the complex pressure output in the outlet tube is denoted by p_3 . The areas of the inlet and outlet tubes are denoted by A_i and A_o , respectively. Although the above three-point method is used in acoustic computation [36], one of the shortcomings of the three-point method is the large discrepancy for higher frequencies at which the one-dimensional inlet pressure calculated by (31) is no longer valid.

Figure 2(b) shows the transmission losses using a one-dimensional model, that is, Equation (32), the original QSRV method with 600 Hz for the center frequency and the present MQSRV method for the three center frequencies (200 Hz, 600 Hz, 1200 Hz), respectively. Although the transmission losses are calculated for every 1 Hz with equal abscissa, only 120 points are plotted for the purpose of illustration. The total DOFs of a FE model discretized by four node elements is 2046, where the number of Krylov subspace bases of both the standard QSRV method and the present MQSRV method is set to only 12 (0.58%). With the present MQSRV method, four Krylov subspace bases are calculated at the three center frequencies to use the same number of Krylov subspace bases as the standard QSRV method. Because the acoustic system and the resulting set of equations are dependent on excitation frequency, larger discrepancies are observed far from the center frequency (600 Hz) with the standard QSRV method in Figure 2(c). In contrast, approximation with the present MQSRV method is accurate for all frequencies. Furthermore, it is important to choose a proper center frequency. To show the effect of the center frequencies, Figure 2(d) shows the transmission loss errors with the two different combinations of center frequencies, that is, [100 Hz, 300 Hz, 500 Hz] and [500 Hz, 700 Hz, 900 Hz]. As expected, the higher accuracy near the center frequencies is obtained. Interestingly, the relative errors predicted by these center frequencies are lower than that of the QSRV method.

The numerical results obtained by the present MQSRV method are several orders of magnitude more accurate than the results obtained by the standard MOR scheme. One of the reasons for these quite significant improvements is that the Krylov subspace bases at the other two center

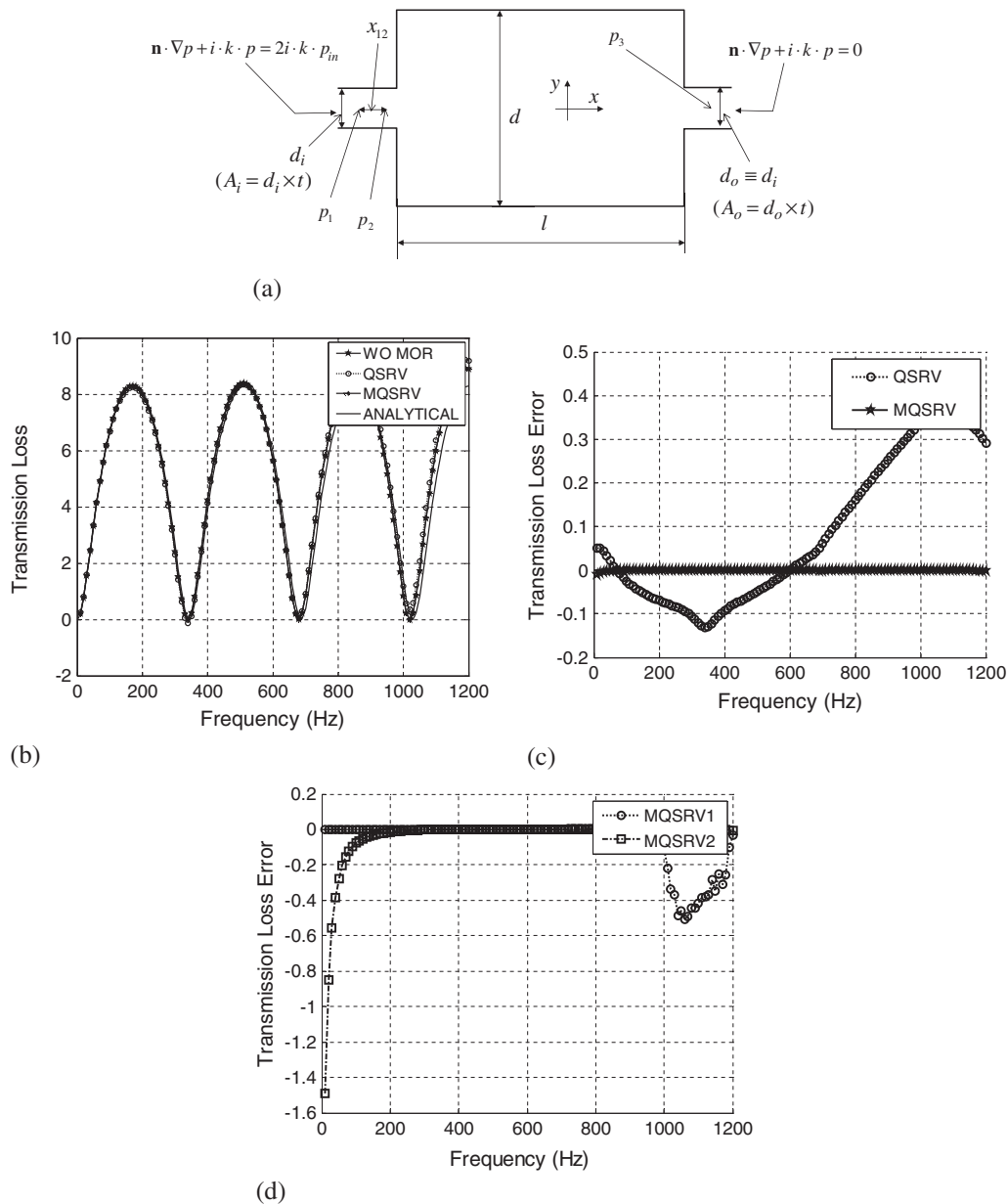


Figure 2. A 2D muffler analysis example. (a) Muffler geometry ($\rho = 1.25 \text{ Kg/m}^3$, $c = 343 \text{ m/s}$, $l = 0.5 \text{ m}$, $d = 0.15 \text{ m}$, $d_i = 0.03 \text{ m}$, $x_{12} = 0.01 \text{ m}$, $t = 1 \text{ m}$, DOFs = 2046, calculated angular velocity = $[0 : 1 : 1200] \text{ (Hz)}$; only 120 points are plotted for the purpose of illustration, the center frequency of QSRV: 600 Hz, the center frequencies of MQSRV: 200 Hz, 600 Hz, 1000 Hz); (b) the calculated transmission loss curves with the existing QSRV method and the present MSQSRV method (total calculation times equal 900.12 s without MOR schemes, 152.52 s by the QSRV method, and 156.31 s by the present MSQSRV method); (c) the transmission loss error curve; and (d) the transmission loss curves with the different center frequencies (MQSRV 1: [100 Hz, 300 Hz, 500 Hz] and MQSRV 2: [500 Hz, 700 Hz, 900 Hz]).

frequencies, that is, 200 Hz and 1000 Hz, 200 Hz and 600 Hz, and 600 Hz and 1000 Hz, also help to improve the approximation accuracy at the one center frequency, that is, 600 Hz, 1000 Hz, and 200 Hz. Without the model order reduction schemes, computation takes approximately 900 s, whereas the standard QSRV method and the present MQSRV method take 152 s and 156 s, respectively. The additional computational time because of the two additional LU factorizations at 200 Hz and 1000 Hz with the present MQSRV method is not significant from a computational point of view.

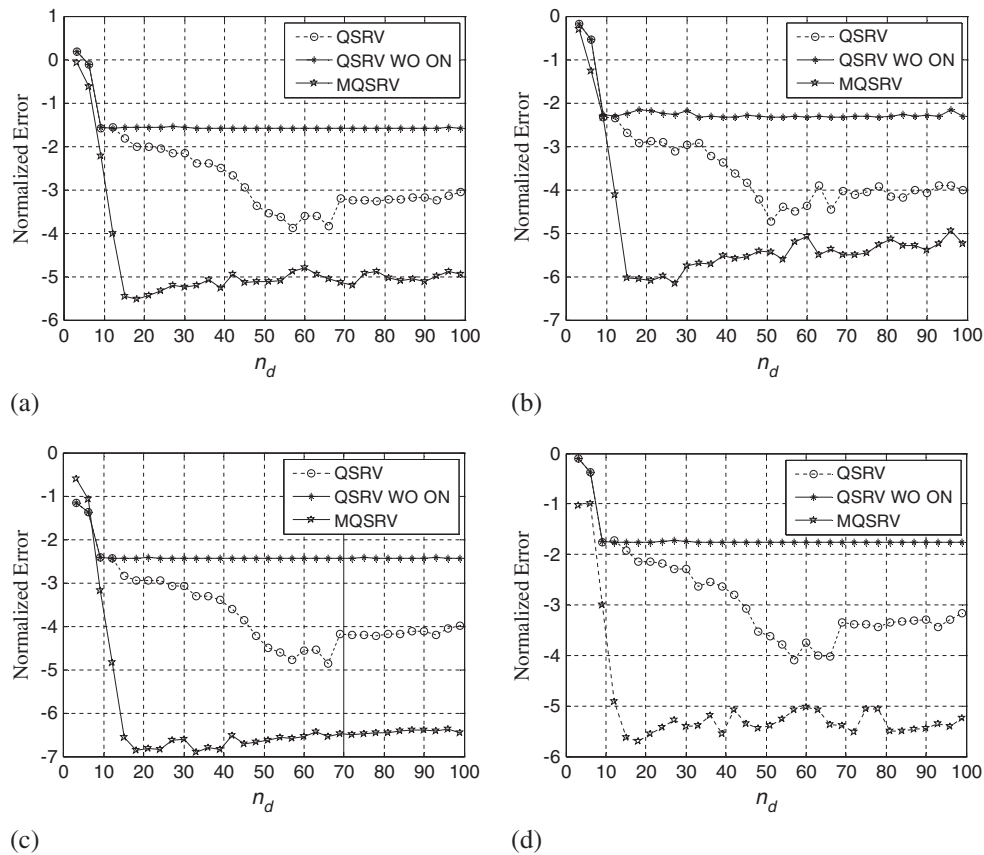


Figure 3. Comparisons of normalized errors: (a) errors for all frequency domains ('QSRV WO ON': the QSRV method without the orthonormal procedure); (b), (c) and (d) normalized errors from 0 Hz to 400 Hz, from 400 Hz to 800 Hz and from 800 Hz to 1200 Hz.

Figure 3 shows improvements in the TL approximations with respect to the number of employed Krylov subspace bases. To show the effect of the orthonormal procedure in the QSRV method, the TL errors without the orthonormal procedure marked by 'QSRV WO ON' in the figure are also presented. As illustrated in Figure 3, the QSRV method without the orthonormal procedure does not improve the approximation accuracy because of the induced truncation error, although the number of bases, that is, the dimension of the vector space, increases. However, compared with the standard QSRV method, the present MQSRV method converges rapidly even without the two mathematical procedures. The rapid convergence seen in Figure 3(a) is also observed for the sub-frequency domains as shown in Figures 3(b), (c), and (d). The numerical accuracy of the present approach with respect to the number of elements (DOFs) is tested in Figure 4. As shown in Figure 4, the developed MQSRV method with 12 basis vectors is very accurate even with the refined finite element meshes. This aspect may be interpreted as the basic concept of the Krylov subspace in [19]. In other words, the n -th polynomial function of response is accurately approximated with the n Krylov subspace bases. Thus, even though the number of DOFs is increased, it is possible to accurately approximate responses.

4.2. Example 2: acoustic example with the Delany–Bazley material model

An expansion chamber similar to the chamber in example 1 with a Delany–Bazley material model is considered in Figure 5 to show the effectiveness of the present method for a fibrous material. Because of the additional attenuation induced by this attached Delany–Bazley layer, higher attenuation of the acoustic pressure is achieved as shown in Figure 5(b). In this example, the transmission

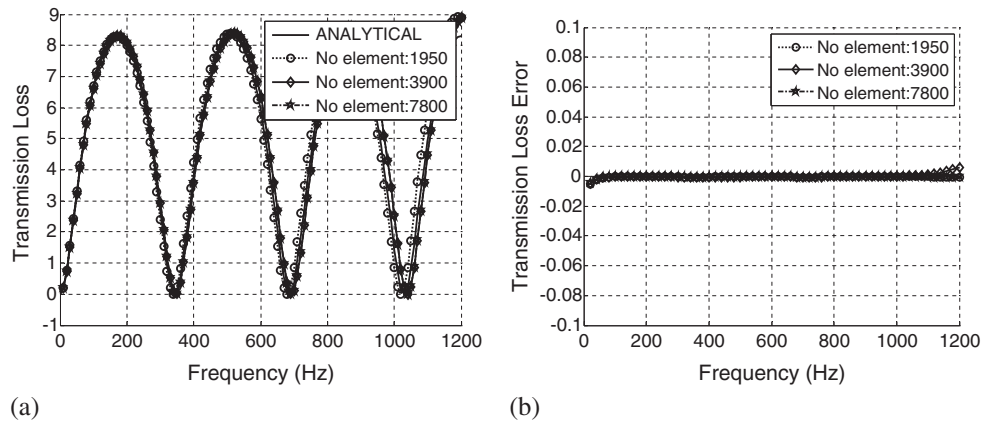


Figure 4. The effect of mesh refinement (the number of the Ritz vectors is fixed to 12). (a) The transmission loss curves for various meshes and (b) the transmission loss errors for various meshes.

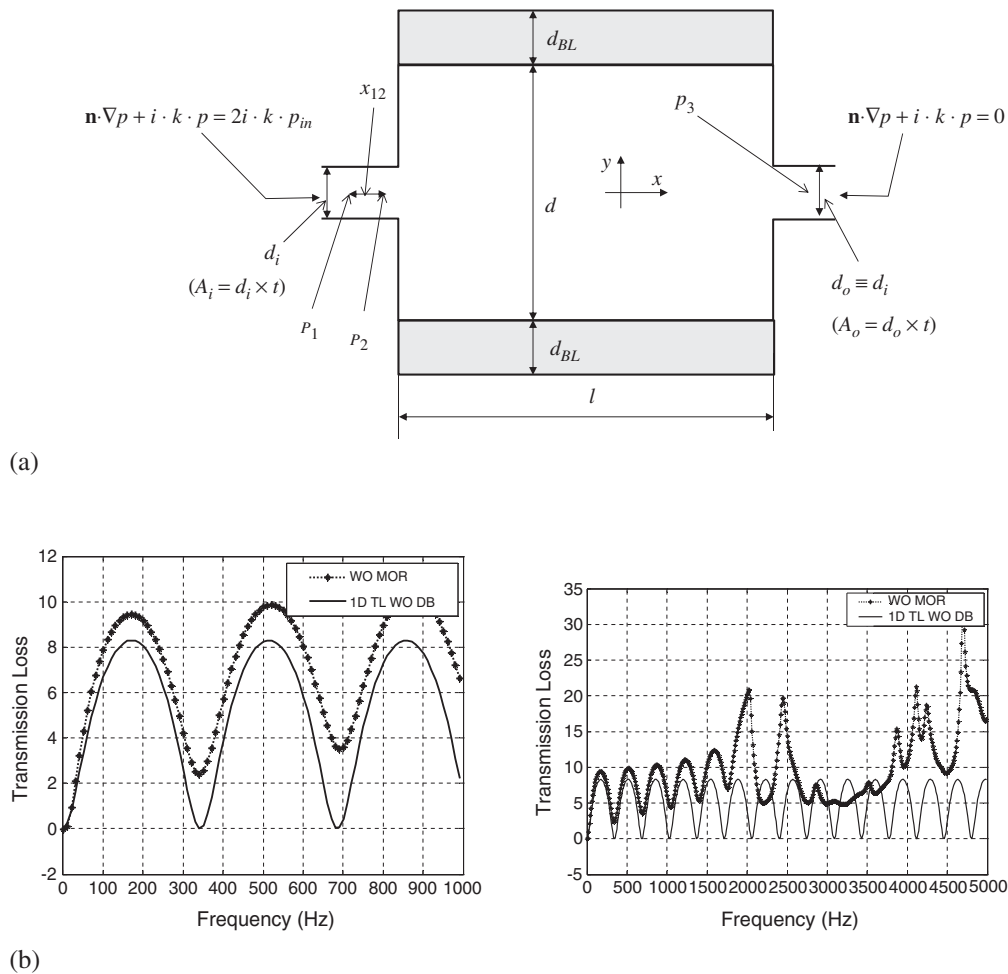


Figure 5. A 2D muffler analysis example with the Delany–Bazley model. (a) Muffler geometry ($\rho = 1.25 \text{ Kg/m}^3$, $c = 343 \text{ m/s}$, $R = 1000$, $l = 0.5 \text{ m}$, $d = 0.15 \text{ m}$, $d_i = 0.03 \text{ m}$, $d_o = 0.01 \text{ m}$, $x_{12} = 0.01 \text{ m}$, $t = 1 \text{ m}$, DOFs = 2310, calculated angular velocity = $[1 : 1 : 5000] \text{ Hz}$; center frequency of QSRV: 600 Hz, center frequencies of MQRV: 200Hz, 600Hz, 1000 Hz); and (b) the transmission loss curves without the MOR method.

loss curve of the higher angular speed domain from 0 Hz to 5000 Hz is considered to further test the characteristics of the present MQSRV method. Large differences between the TL with direct finite element analysis and the TL assuming a one-dimensional acoustic wave exist in Figure 5(c). As in example 1, the TL curves obtained with the QSRV method and the present MQSRV method are calculated in Figure 6 using the three center angular speeds (5000/6 Hz, 2500 Hz, $5000 \times 5/6$ Hz) for the MQSRV method and one center angular speed (2500 Hz) for the QSRV method with 30 Krylov subspace bases. The present MQSRV method converges rapidly as shown in Figure 6(a). Despite the superior convergence of the present method, there are some differences because of the insufficient

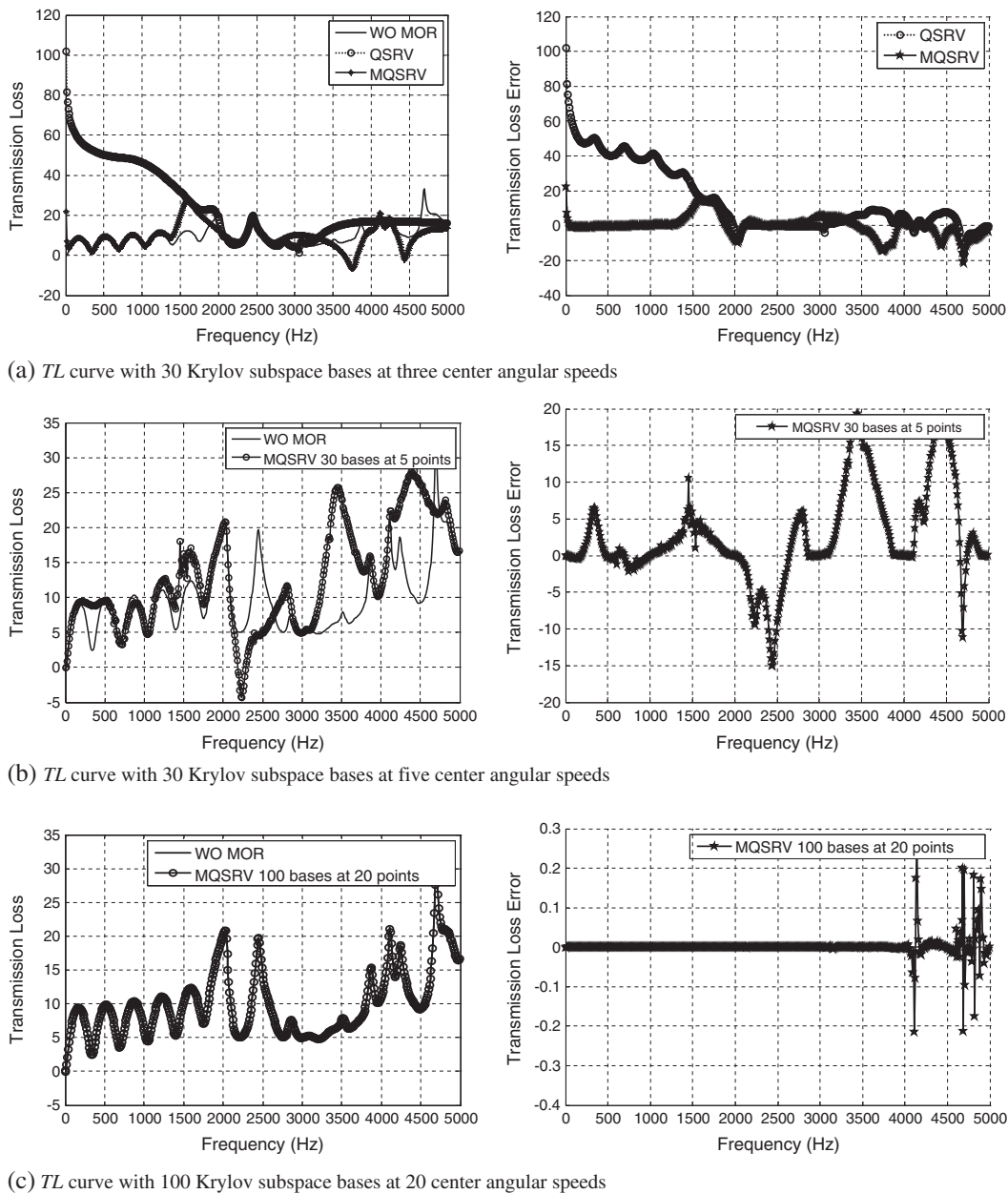


Figure 6. The effect of varying the number of Krylov subspace bases and center angular speeds with the present MQSRV method on convergence improvement. (a) TL curve with 30 Krylov subspace bases at three center angular speeds (calculation time: without MOR scheme, 7666.2 s; QSRV, 270.5 s; MQSRV, 299.2 s); (b) TL curve with 30 Krylov subspace bases at five center angular speeds (calculation time: 292.8 s); and (c) TL curve with 100 Krylov subspace bases at 20 center angular speeds (calculation time: 533.5 s).

vector space of the Krylov subspace bases. At this stage, three approaches to improve the convergence are imaginable. First, it is possible to increase the number of Krylov subspace bases used for maintaining the number and location of the three center angular speeds. The addition of more center angular speeds while maintaining the number of Krylov subspace bases is also possible. Furthermore, it may be possible to combine the two approaches. Figures 6(b) and (c) shows the results of the approaches mentioned with equally distributed center frequencies for the MQSRV method.

4.3. Example 3: three-dimensional chamber example

For the next numerical example, let us consider the chamber shown in Figure 7 [36]. This 3D structure without a stinger has a transmission loss curve similar to the first numerical example. Thus, the transmission loss is calculated by the three-point method. The detailed geometry of the 3D expansion chamber is shown in Figure 7(a). The *TL* curves of each MOR method are plotted in Figure 8.

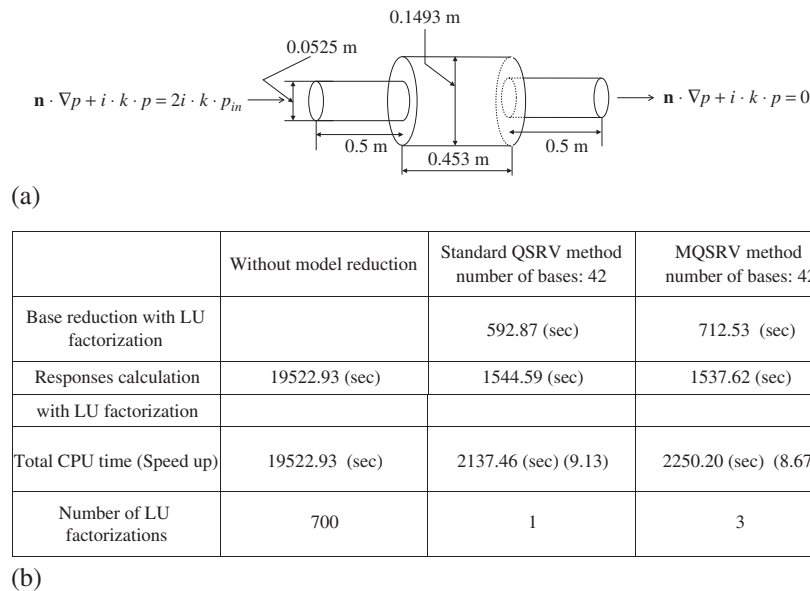


Figure 7. A 3D chamber example: (a) geometry and FE mesh of a 3D chamber and (b) the time comparison among the methods.

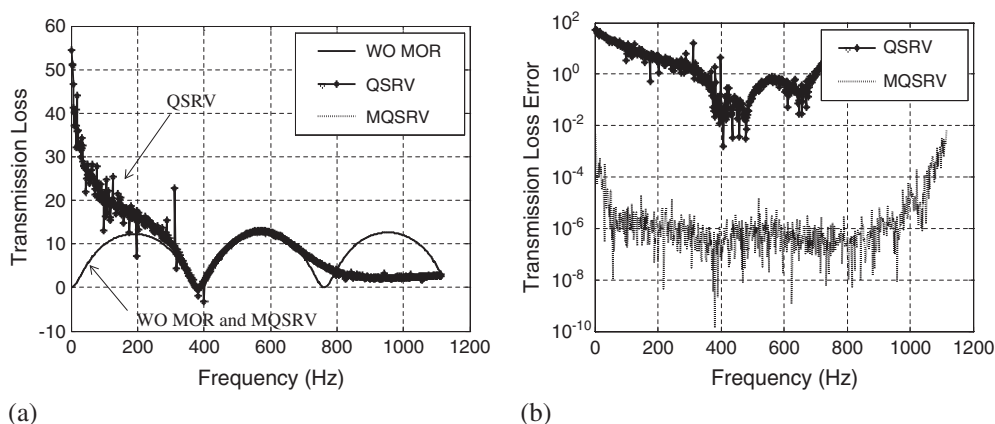


Figure 8. (a) Transmission loss curves for angular speed domains from 0 Hz to 1114 Hz (7000 rad/s). WO MOR, transmission loss without the MOR method; QSRV, transmission loss with the standard RV method (center angular speed, 500 Hz (3144 rad/s)); MQSRV, transmission loss with the present multifrequency quasi-static RV method (center angular speeds: 167, 500, 834 Hz) and (b) Transmission loss error curves.

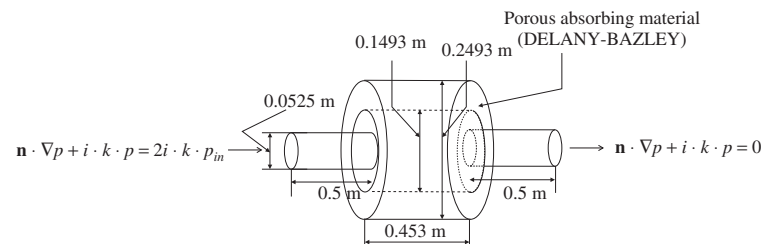
Figure 7(b) summarizes the calculation times without the MOR scheme and with the QSRV and MQSRV methods with 700 equal sampling points from 0 (rad/s) to 7000 (rad/s). For the MQSRV method, the three center angular speeds, 1049.29, 3144, 5240.17 (rad/s), are used. Consequently, three LU factorizations are required for the MQSRV method where only one LU factorization is used for the standard QSRV method. Therefore, it takes more time for the MQSRV method to calculate its bases (Figure 7(b)). However, the prediction from the MQSRV method is much more accurate than that of the QSRV method (Figure 8).

4.4. Example 4: three-dimensional chamber example with Delany–Bazley material model

In the next numerical example, the 3D chamber problem Figure 9 is reconsidered with the Delany–Bazley material model of Equation (4). Except for the attached outer fibrous absorbing material, it has the same geometry and material properties as the previous example. Because of this attached fibrous absorbing layer, the transmission loss curve of this structure is altered as shown in Figure 10(a). In the MQSRV method, the equally distributed 14 center frequencies are due to the complex response and nature of the model. As expected, the overall transmission loss level is increased. As in the previous examples, the QSRV method is not effective as shown in Figure 10(b), but the present MQSRV method provides an accurate transmission curve as shown in Figures 10(c) and (d).

4.5. Example 5: three-dimensional acoustic muffler

As the last numerical example, a 3D acoustic muffler is considered (Figure 11). Compared with the configuration of the first example, the configuration of pipes and expansion chambers become more complex. The total number of FE elements is 773,546 and the total DOF is 1,101,787. In a workstation computer (i7 960 Bloomfield, 4 Cores, 24 GB memory), it takes approximately 76 s to calculate pressure responses for a specific excitation frequency. Thus, the total computation time to calculate the frequency response is approximately 91,873 s (approximately 25 h); several computers are used to calculate the frequency response without the model reduction scheme.



(a)

	Without model reduction	Standard QSRV method number of bases: 42	MQSRV method number of bases: 42
Base reduction with LU factorization		1324.68 (sec)	2797.54 (sec)
Response calculation with LU factorization	83540.8 (sec)	2720.67 (sec)	3044.71 (sec)
Total CPU time (Speed up)	83540.8 (sec)	4045.50 (sec) (20.65)	5842.25 (sec) (14.29)
Number of LU factorizations	700	1	14

(b)

Figure 9. The 3D chamber example with porous absorbing material (flow resistance R : 1424, number of elements: 122,356, DOFs: 174,604): (a) geometry and FE mesh of a 3D chamber and (b) time comparison among the methods.

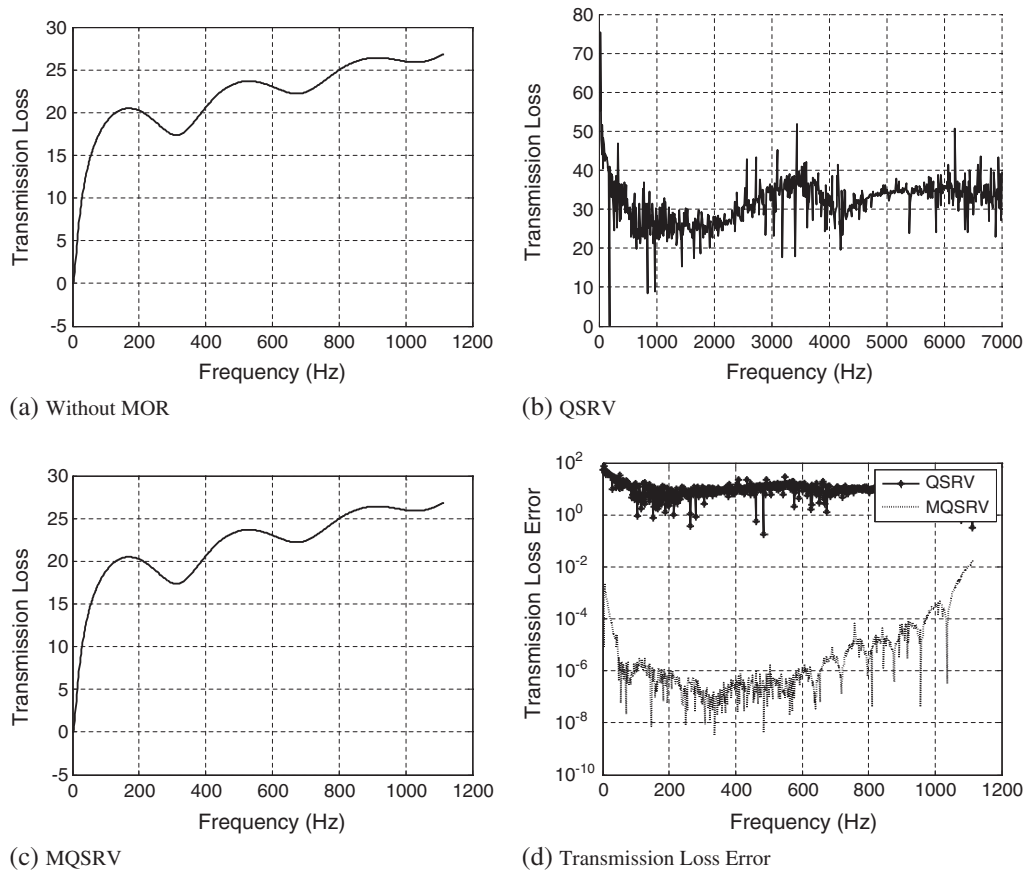


Figure 10. A comparison with 42 bases of the 3D structure with the fibrous absorbing material. The responses (a) without MOR, (b) with QSRV, (c) with MQSRV, and (d) transmission loss errors.

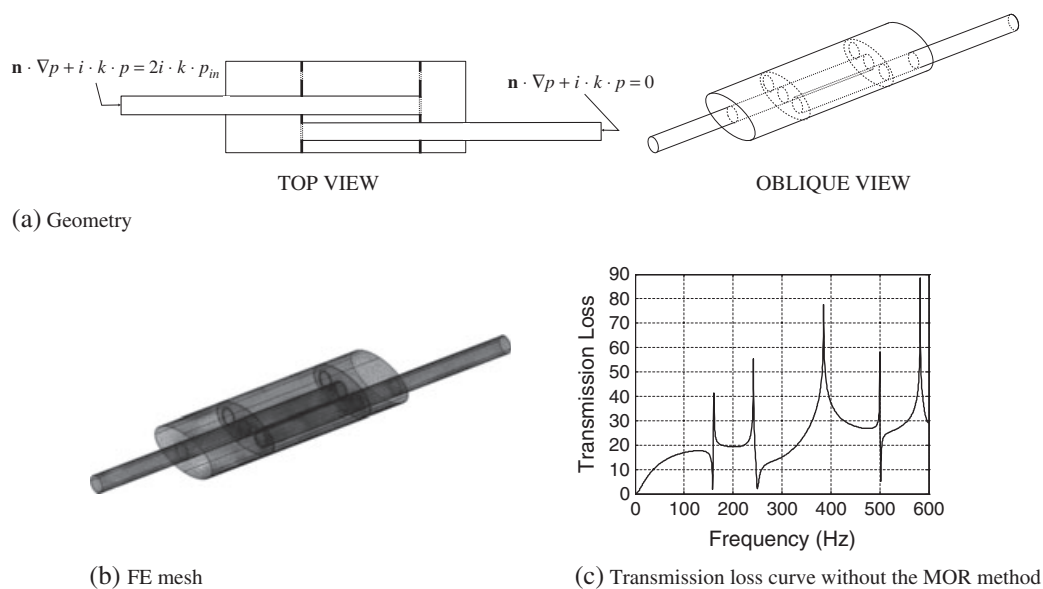


Figure 11. A three-dimensional acoustic muffler example.

Because of the boundary conditions, the stiffness, mass matrices and force vector become frequency-dependent. Figure 12 shows the transmission loss curves with the existing and developed MOR schemes. As a numerical test, the transmission curve for a frequency domain from 0 Hz to 600 Hz is calculated for every 0.5 Hz. For the MQSRV method, we equally distribute the 12 center frequencies. As shown, the conventional RV method with 120 bases is not effective in this example, whereas the present MQSRV method is very effective, even with 24 bases. As stated in the previous section, issues remain with respect to choosing the proper number and locations of center frequencies for the MQSRV method. This issue is also problematic for the existing QSRV method. On the basis of our experience, the use of one to three center frequencies between two resonance frequencies or peaks is optimal. However, this rule may be hard to apply in practice because resonance frequencies or peaks are unknown in prior. Thus, we suggest using evenly distributed center frequencies and increasing the number of Krylov subspace bases incrementally.

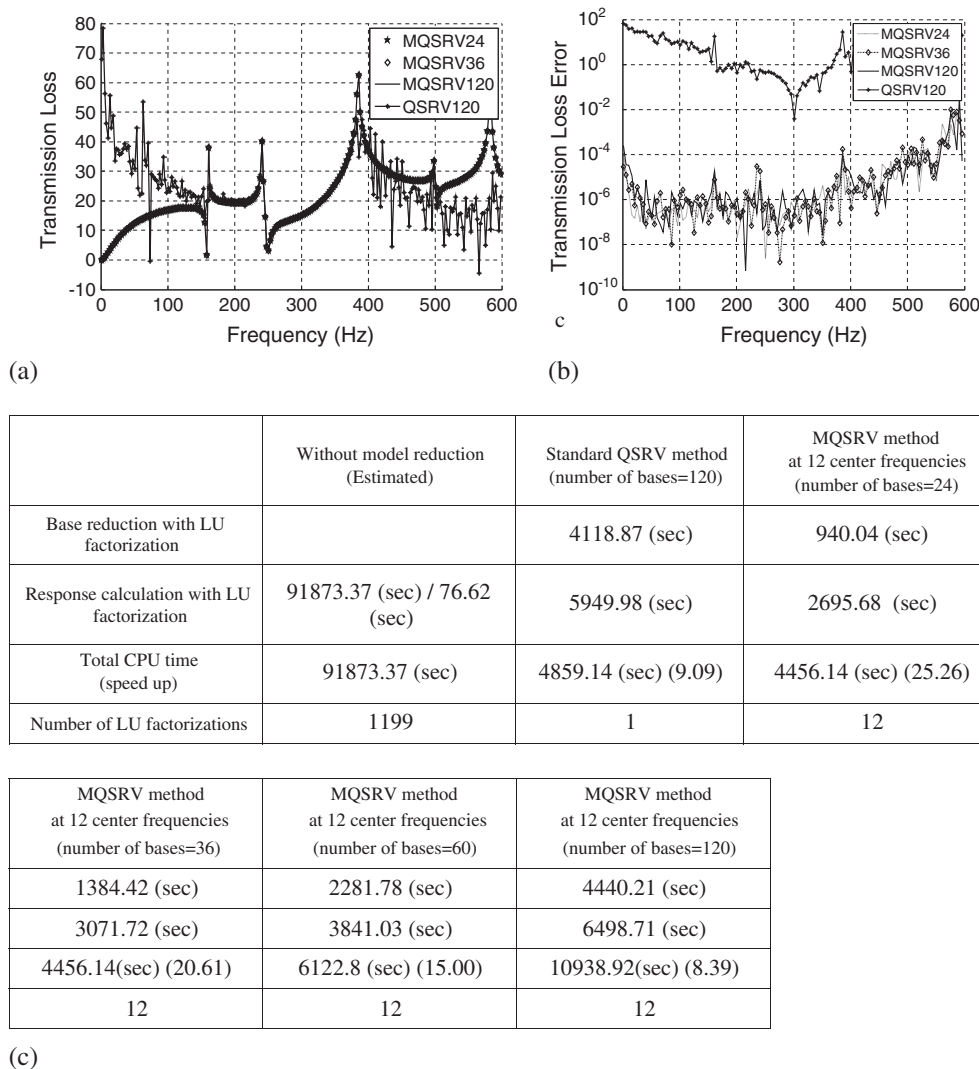


Figure 12. A comparison among the existing and developed MOR schemes: (a) *TL* curves of the QSRV method with 300 Hz center frequency and the MSRV method with 12 center frequencies for every 50 Hz and 10 bases for each center frequency; (b) the absolute error curves of the approximated *TL* curves (only the absolute errors at 120 points are plotted); and (c) comparison of the computation time.

5. CONCLUSIONS

Calculating acoustic and vibration responses by means of a FE procedure is important. The active DOFs of a complex FE model are often reduced by applying a MOR scheme to accelerate the solution procedure with limited computational resources. When an engineering system becomes frequency-independent (constant or linear system), existing MOR methods such as the Guyan reduction method, the MS method, the RV method, and the QSRV method [2] can efficiently calculate acoustic and vibration responses without any computational problems. In contrast, when an engineering system becomes frequency-dependent, the way in which to apply these established MOR methods effectively is unclear. In an effort to develop a MOR method for a time-dependent or frequency-dependent system, this research presents a modified MOR method, called the MQSRV method, which is based on the QSRV method. By extending the concepts of the established QSRV method in [2], this method calculates the Krylov subspace bases at multiple center frequencies without an orthonormal procedure.

On the basis of an investigation of the details of the established RV and QSRV methods, we can conclude that the orthonormal procedure usually employed to enhance the mathematical properties of the Krylov subspace bases is not essential, at least from an engineering point of view. Although an orthogonalization procedure such as the Arnoldi process makes the calculated bases orthogonal to each other, the two vector spaces of the unorthogonalized bases and the orthogonalized bases should be mathematically identical to each other. Accumulated numerical errors such as truncation error may cause them to differ in practice. Furthermore, because the normalization procedure does not change the vector space either, it can also be omitted. However, these omissions do not improve the computational speed much.

In conclusion, the proposed scheme achieves a significant gain in computational efficiency, as well as enhanced accuracy in comparison with the existing MOR scheme. Through several acoustic analysis examples, we found that higher speed-ups can be achieved with the established MQSRV method for frequency-dependent acoustic systems. One of the remaining issues of the present MQSRV method is establishing effective and systematic approaches for center frequencies and determining the optimal number of Krylov subspace bases associated with the center frequencies. We suggest using one to three evenly distributed center frequencies and increasing the number of Krylov subspace bases incrementally while monitoring the accuracy of solutions. Future research may allow for the application of the developed MQSRV method to optimize size and topology for acoustic design with and without porous and absorptive material.

APPENDIX A: ORTHOGONALITY

To show the mathematical characteristics of the present MQSRV method, let us consider a linear system of (A.1) and (A.2).

$$\mathbf{K}_c = \begin{bmatrix} 2k & -k \\ -k & 2k \end{bmatrix}, \mathbf{M}_c = \begin{bmatrix} m & 0 \\ 0 & 2m \end{bmatrix}, \mathbf{F}_c = \begin{bmatrix} 0 \\ 1 \end{bmatrix} \quad (\text{A.1})$$

$$[\mathbf{K}_c - \omega^2 \mathbf{M}_c] \mathbf{X} = \mathbf{F}_c. \quad (\text{A.2})$$

The eigenvalues of the above system are calculated as follows:

$$\omega_{\text{eigen},1} = 0.7962 \sqrt{\frac{k}{m}}, \quad \omega_{\text{eigen},2} = 1.5382 \sqrt{\frac{k}{m}}. \quad (\text{A.3})$$

To illustrate the orthogonality of the calculated bases, the angles of the basis vectors are calculated with respect to the center frequency from 0 (rad/s) to 2 (rad/s) and are plotted in Figure A.1. Here, m and k are set to be 1. As shown, the bases calculated by the QSRV method are orthogonal to each other in Figure A.1(a) whereas the bases calculated by the present MQSRV method are bi-orthogonal in Figure A.1(b). Interestingly, because of the truncation errors, that,

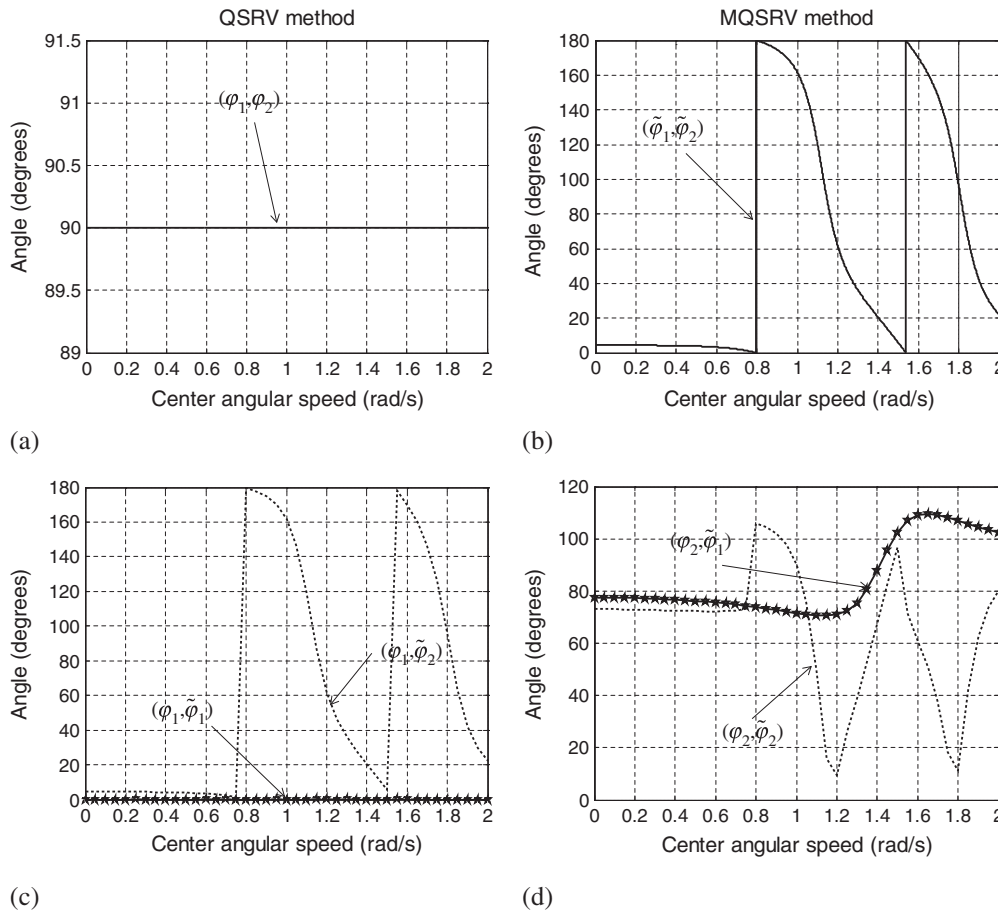


Figure A.1. The angles of the Krylov subspaces of the QSRV and MQSRV methods. φ_1 and φ_2 : the bases of the QSRV method; $\tilde{\varphi}_1$ and $\tilde{\varphi}_2$: the bases of the MQSRV method.

$|\mathbf{K}_c - \omega_{\text{eign},1}^2 \mathbf{M}_c| \approx 0$, $|\mathbf{K}_c - \omega_{\text{eign},2}^2 \mathbf{M}_c| \approx 0$, the bases derived with the present MQSRV method appear to lose orthogonality in Figure A.1(b), but they are actually pointing in different directions (see Figures A.1(c) and (d)). As expected, φ_1 and $\tilde{\varphi}_1$ point in the same direction. In Figure A.1(d), the angle between φ_2 and $\tilde{\varphi}_1$ does not become zero, which indicates that the direct Krylov subspace bases of $\tilde{\varphi}_1$ and $\tilde{\varphi}_2$ are bi-orthogonal and represent the two-dimensional vector space.

ACKNOWLEDGEMENTS

The author acknowledges the support from the Basic Science Research Program through the National Research Foundation of Korea (NRF) funded by the Ministry of Education, Science and Technology (2010-0028152).

REFERENCES

1. Wilson EL. A new method of dynamic analysis for linear and nonlinear systems. *Finite Elements in Analysis and Design* 1985; **1**:21–23.
2. Gu JM, Ma ZD, Hulbert GM. A new load-dependent Ritz vector method for structural dynamics analyses: quasi-static Ritz vectors. *Finite Elements in Analysis and Design* 2000; **36**:261–278.
3. Han JS, Muller C, Wallrabe U, Korvink JG. Design, simulation, and fabrication of a quadstable monolithic mechanism with X- and Y-directional bistable curved beams. *Journal of Mechanical Design* 2007; **129**:1198–1203.
4. Yoon GH. Structural topology optimization for frequency response problem using model reduction schemes. *Computer Methods in Applied Mechanics and Engineering* 2010; **199**:1744–1763.

5. Yao MS. Nonlinear structural dynamic finite element analysis using Ritz vector reduced basis method. *Shock and Vibration* 1996; **3**:259–268.
6. Bottasso CL, Croce A, Savini B, Sirchi W, Trainelli L. Aero-servo-elastic modeling and control of wind turbines using finite-element multibody procedures. *Multibody System Dynamics* 2006; **16**:291–308.
7. Jackson T, Livne E. Design-oriented structural-model order reduction of strain-actuated flight-vehicle structures. *Journal of Aircraft* 2006; **43**:182–188.
8. Wittig T, Schuhmann R, Weiland T. Model order reduction for large systems in computational electromagnetics. *Linear Algebra and its Applications* 2006; **415**:499–530.
9. Ma O, Wang JG. Model order reduction for impact-contact dynamics simulations of flexible manipulators. *Robotica* 2007; **25**:397–407.
10. Ma ZD, Kikuchi N, Hagiwara I. Structural topology and shape optimization for a frequency-response problem. *Computational Mechanics* 1993; **13**:157–174.
11. Ma Z-D, Kikuchi N, Cheng H-C, Hagiwara I. Topological optimization technique for free vibration problems. *Journal of Applied Mechanics* 1995; **62**:200–207.
12. Guyan RJ. Reduction of stiffness and mass matrices. *AIAA Journal* 1964; **3**:380.
13. Craig RR, Ni ZH. Component mode synthesis for model order reduction of nonclassically damped systems. *Journal of Guidance Control and Dynamics* 1989; **12**:577–584.
14. Artemyev BN, Buntov VD, Komarov VM, Sivers MA. Order reduction methods for model-equations of oscillatory circuit systems. *Izvestiya Vysshikh Uchebnykh Zavedenii Radioelektronika* 1985; **28**:38–45.
15. Gu JM, Ma ZD, Hulbert GM. Quasi-static data recovery for dynamic analyses of structural systems. *Finite Elements in Analysis and Design* 2001; **37**:825–841.
16. Morris AS. Simplified technique of model order reduction with performance verification by fast digital-simulation. *IEE Proceedings-D Control Theory and Applications* 1984; **131**:69–73.
17. Bathe KJ. *Finite Element Procedures*. Prentice Hall: New Jersey, 1996.
18. Kale I, Mackenzie JP, Laakso TI. Motor car acoustic response modelling and order reduction via balanced model truncation. *Electronics Letters* 1996; **32**:965–966.
19. Watanabe T, Asai H. Macromodel generation for hybrid systems consisting of electromagnetic systems and lumped RLC circuits based on model order reduction. *IEICE Transactions on Fundamentals of Electronics Communications and Computer Sciences* 2004; **E87a**:398–405.
20. Han JS, Rudnyi EB, Korvink JG. Efficient optimisation of transient dynamic problems in MEMS devices using model order reduction. *Journal of Micromechanics and Microengineering* 2005; **15**:822–832.
21. Lee SH, Huang TY, Wu RB. Fast waveguide eigenanalysis by wide-band finite-element model-order reduction. *IEEE Transactions on Microwave Theory and Techniques* 2005; **53**:2552–2558.
22. Wu H, Cangellaris AC. Krylov model order reduction of finite element approximations of electromagnetic devices with frequency-dependent material properties. *International Journal of Numerical Modelling-Electronic Networks Devices and Fields* 2007; **20**:217–235.
23. Remis R. An efficient model-order reduction approach to low-frequency transmission line modeling. *Progress in Electromagnetics Research* 2010; **101**:139–155.
24. Srinivasan Puri R. *Krylov Subspace Based Direct Projection Techniques for Low Frequency, Fully Coupled, Structural Acoustic Analysis and Optimization*. Oxford Brookes University: Oxford, 2008.
25. Heres PJ. *Robust and Efficient Krylov Subspace Methods for Model Order Reduction*. Eindhoven University of Technology: Eindhoven, 2005.
26. Hili M, Fakhfakh T, Haddar M. Failure analysis of a misaligned and unbalanced flexible rotor. *Journal of Failure Analysis and Prevention* 2006; **6**:73–82.
27. Orlanski I. A simple boundary condition for unbounded hyperbolic flows. *Journal of Computational Physics* 1976; **21**:251–269.
28. Kinsler LE. *Fundamentals of Acoustics*, (3rd edn) Wiley: New York, 1982.
29. Fouladi MH, Ayub M, Nor MJM. Analysis of coir fiber acoustical characteristics. *Applied Acoustics* 2011; **72**:35–42.
30. Alba J, Ramis J, Lorenzana MT, del Rey R. Proposal a empirical model for absorbent acoustical materials. *Revista Internacional de Metodos Numericos para Calculo y Diseno en Ingenieria* 2008; **24**:147–162.
31. Mike Y. Acoustic properties of porous materials -generalizations of empirical models. *The Acoustical Society of Japan* 1990; **11**:25–28.
32. Delany ME, Bazley EN. Acoustical properties of fibrous absorbent materials. *Applied Acoustics* 1970; **3**:105–116.
33. Allard JF, Champoux Y. New empirical equations for sound-propagation in rigid frame fibrous materials. *Journal of the Acoustical Society of America* 1992; **91**:3346–3353.
34. Song ZF, Su DL, Duval F, Louis A. Model order reduction for Peec modeling based on moment matching. *Progress in Electromagnetics Research* 2011; **114**:285–299.
35. Munjal ML. *Acoustics of Ducts and Mufflers with Application to Exhaust and Ventilation System Design*. Wiley: New York, 1987.
36. Bilawchuk S, Fyfe KR. Comparison and implementation of the various numerical methods used for calculating transmission loss in silencer systems. *Applied Acoustics* 2003; **64**:903–916.